Journal of Mineralogical and Petrological Sciences, Volume 98, page 215-234, 2003

Compressibility of phase A, $Mg_7Si_2H_6O_{14}$ up to 11.2 GPa

Takahiro KURIBAYASHI*, Yasuhiro KUDOH* and Hiroyuki KAGI**

*Institute of Mineralogy, Petrology and Economic Geology, Graduate School of Science, Tohoku University, Sendai 980-8578, Japan
**Laboratory for Earthquake Chemistry, Faculty of Science, University of Tokyo, 113-0033, Japan

A single crystal high-pressure X-ray diffraction study of phase A was performed using a diamond anvil cell up to 11.2 GPa at ambient temperature. The chemical formula of this sample, determined by EPMA from an average of 18 data points, was $Mg_{6.99}Si_{1.99}H_{6.06}O_{14}$. Axial linear compressibilities of phase A were β_a=2.92(2) and β_c= 2.17(3) ($\times 10^{-3}$/GPa). The isothermal bulk modulus, calculated using the Birch-Murnaghan equation of state, was K_{T0}=105(4) GPa with a pressure derivative K'=3.9(8) and V_0=512.2(6) Å^3. The bulk modulus correlates with the summation of the filling factor of the tetrahedral site and the octahedral site, as shown for the minerals on the forsterite-brucite join in the system MgO-SiO_2-H_2O.

Introduction

Ringwood and Major (1967) studied experimentally the system of Mg_2SiO_4-MgO-H_2O in order to clarify its phase relations under high temperature and pressure conditions. They discovered new types of hydrous magnesium silicate minerals. They denoted these minerals as phase A, phase B and phase C. Kanzaki (1991) has been reported later that phase C is the same phase as super hydrous phase B. Yamamoto and Akimoto (1974; 1977) investigated the phase relationships in the system MgO-SiO_2-H_2O (MSH) under pressures between 2.9 GPa and 7.7 GPa and at temperatures between 500°C and 1200°C. Then they determined the lower stability limits of phase A and OH-chondrodite (OH-chondrodite was originally denoted as phase D in their study). Phase equilibrium in the MSH system has recently been reinvestigated to study the stability fields of humite minerals and phase A (ex. Burnley and Navrotsky, 1996; Wunder, 1998; Pawley, 2000). These studies showed that the stability fields of phase A, OH-chondrodite and OH-clinohumite expanded higher pressure regions. Ulmer and Trommsdorff (1994) showed the breakdown of antigorite, which produced enstatite + phase A at pressures > 6.6 GPa and at temperatures > 550 °C. Phase A may play an important role in hydration and dehydration processes in subduction zones as a reservoir and a carrier of water. The presence of water in the structure of a mineral may also change its physical properties (for example, bulk modulus and elastic constants). The isothermal bulk moduli of minerals are closely related to the bulk sound velocity of seismic wave. For this reason, bulk moduli of minerals need to be investigated.

Parise et al. (1998) showed a simple positive correlation between isothermal bulk modulus (K) versus density (ρ) for dense hydrous magnesium silicate minerals (DHMS) and hydroxides. However, Pawley et al. (1995) reported an isothermal bulk modulus of phase A (K_{T0}=145(5) GPa, assuming K'=4) from high-pressure powder X-ray diffraction with a diamond anvil cell (DAC). This value is significantly higher than that of forsterite (K_{T0}=122.6 GPa, Kudoh and Takeuchi, 1985; K_{T0}=125(2) GPa with K'=4.0(4), Downs et al., 1995) although the density of phase A (2.96 g/cm^3) is lower than that of forsterite (3.22 g/cm^3). Similarly, Faust and Knittle (1994) reported the isothermal bulk modulus of natural chondrodite (K_{T0}=136.2(8.8) GPa with a pressure derivative K'=3.7(4)) from high-pressure powder X-ray diffraction using a DAC. This value is also slightly higher than that of forsterite. These minerals on the forsterite-brucite join in the MSH system showed differences from these characteristic relationships in physical properties. The crystal structure of phase A, which is different from those of humite minerals such as OH-chondrodite and OH-clinohumite, might be caused to this irregular relation, although the chemical formula of phase A, $2Mg_2SiO_4 \cdot 3Mg(OH)_2$ is similar to those of humite minerals, $mMg_2SiO_4 \cdot Mg(OH)_2$ (m=1-4). On the other hand, Sinogeikin and Bass (1999) determined the elastic constants of natural chondrodite (ρ=3.227(10) g/cm^3) using the Brillouin scattering method and reported a Ks of 118.2(2) GPa, which was lower than

T. Kuribayashi, t-kuri@mail.tains.tohoku.ac.jp Corresponding author
Y. Kudoh, ykudoh@mail.tains.tohoku.ac.jp
H. Kagi, kagi@eqchem.s.u-tokyo.ac.jp

that of forsterite. Moreover, Ross and Crichton (2001) reported the isothermal bulk modulus of OH-chondrodite and OH-clinohumite to be K_{T0}=115.7(8) GPa with K'= 4.9(2) and K_{T0}=119.4(7) with K'=4.8(2) using high-pressure single crystal X-ray diffraction. Kuribayashi et al. (1999) reported the isothermal bulk modulus of phase A was K_{T0}=104.8(4.0) GPa with K'=4.4(1.1). Compared to the results of Crichton and Ross (2002) and Ross and Crichton (2001), who reported a bulk modulus of phase A (K_{T0}=97.5(4) GPa with K'=5.97(14)) and that of OH-chondrodite and OH-clinohumite, these results are at odds with the earlier studies. It is important crystallographically to resolve this problem in order to understand the compression mechanism of homologous series minerals such as phases on the forsterite-brucite join in the MSH system under high-pressure conditions. In this paper, we report the compression and the crystal structure data of phase A under high-pressure conditions up to 11.2 GPa to understand the effect of pressure on its crystal structure. Compared to the humite minerals, which have similar chemical compositions, the compression mechanism of minerals in the forsterite-brucite join is discussed.

Experimental procedure

The sample used for this study was synthesized at 10 GPa, 1000°C in the USSA 2000 uniaxial split-sphere apparatus at SUNY Stony Brook (Kagi et al., 2001). The Mg/Si ratio of this sample was 3.51, as determined by EPMA analysis (JEOL, JXA-8800M) and its chemical formula, averaged by 18 data points, was $Mg_{6.99}Si_{1.99}H_{6.06}O_{14}$. Hydrogen content was estimated by the deficit from total weight. A single crystal of phase A (60×50×30 μm in size) was used for all X-ray diffraction measurements. A modified Merrille-Bassett type diamond anvil cell (Kudoh and Takeda, 1986) was used for the high-pressure experiment. The SUS301 stainless steel plate with a 200 μm diameter hole in the center was used as a gasket. A 4:1 fluid mixture of methanol and ethanol was used for the pressure medium. Pressure at each data point was determined by the ruby fluorescence method (Piermarini et al.,

Table 1. Variations of each cell parameter of phase A with pressure up to 11.2 Gpa

GPa	a (Å)	c (Å)	V (Å^3)
0.0	7.8604 (7)	9.5702 (8)	512.1 (1)
3.6	7.768 (1)	9.496 (4)	496.2 (3)
4.4*	7.751 (1)	9.475 (2)	493.0 (2)
6.2	7.708 (1)	9.435 (5)	485.4 (3)
6.4	7.706 (1)	9.427 (4)	484.8 (3)
9.1	7.649 (1)	9.381 (5)	475.3 (3)
9.4*	7.644 (1)	9.372 (1)	474.2 (2)
9.6	7.640 (1)	9.373 (5)	473.8 (3)
10.8	7.624 (1)	9.347 (4)	470.5 (2)
11.2	7.607 (1)	9.339 (7)	468.0 (4)

* Results of 2nd run using the same sample with another orientation in DAC.

Table 2. Structural refinement information and latest R and R_w value of phase A at each pressure

Pressure	0	3.6	4.4*	6.2	9.1	9.4*	10.8
Scan method	ω–2θ	ω–2θ	ω–2θ	ω–2θ	ω–2θ	ω–2θ	ω–2θ
Collected reciprocal region	h+,k+,l±	h+,k±,l±	h±,k±,l±	h+,k±,l±	h+,k±,l±	h±,k±,l±	h±,k±,l±
Measured reflections	1204	4138	3115	4083	4129	2986	2859
Reflections for analysis	378	97	104	83	81	105	102
Number of variable	34	33	28	30	29	29	31
Space group	$P6_3$	$P6_3$	$P6_3$	$P6_3$	$P6_3$	$P6_3$	$P6_3$
R and R_w	5.6	6.4	8.1	6.7	9.3	6.8	6.2
	4.8	6.4	8.6	6.8	9.2	7.5	6.3

* Results of 2nd run using the same sample with another orientation in DA.

$R=\Sigma||Fo|-|Fc||/\Sigma|Fo|$

$R_w=(\Sigma w\,(|Fo|-|Fc|)^2/\Sigma w\,Fo^2)^{(1/2)}$

Table 3. Final atomic coordinates of phase A at each pressure condition

		0.0		3.6		4.4*		6.2		9.1		9.4*		10.8	
Si1	x	0.6667		0.6667		0.6667		0.6667		0.6667		0.6667		0.6667	
	y	0.3333		0.3333		0.3333		0.3333		0.3333		0.3333		0.3333	
	z	0.1790	(8)	0.1932	(107)	0.1847	(91)	0.1928	(119)	0.1712	(150)	0.1834	(90)	0.1950	(84)
	Biso	0.60	(6)	1.1	(4)	0.0		1.7	(6)	0	(4)	0.2	(3)	0.1	(3)
Si2	x	0		0		0		0		0		0		0	
	y	0		0		0		0		0		0		0	
	z	0.4062	(6)	0.4293	(97)	0.4097	(64)	0.4184	(165)	0.3571	(107)	0.4048	(82)	0.4117	(96)
	Biso	0.63	(5)	0.8	(3)	0.0		0.9	(4)	0.7	(4)	1.4	(4)	0.8	(3)
Mg1	x	0.3720	(3)	0.3731	(17)	0.3730	(22)	0.3713	(20)	0.3710	(24)	0.3768	(18)	0.3754	(15)
	y	0.4558	(3)	0.4566	(22)	0.4560	(26)	0.4536	(25)	0.4555	(28)	0.4587	(21)	0.4577	(17)
	z	0.3902	(5)	0.4076	(74)	0.3929	(61)	0.3837	(92)	0.3639	(83)	0.3885	(57)	0.3844	(59)
	Biso	0.60	(4)	1.2	(3)	1.1	(3)	1.3	(3)	0.6	(3)	0.6	(2)	1.1	(2)
Mg2	x	0.2231	(3)	0.2243	(21)	0.2207	(23)	0.2235	(26)	0.2215	(33)	0.2169	(20)	0.2178	(15)
	y	0.2437	(3)	0.2485	(19)	0.2436	(20)	0.2485	(23)	0.2456	(28)	0.2432	(20)	0.2455	(12)
	z	0.1159	(4)	0.1373	(78)	0.1141	(47)	0.1093	(110)	0.1116	(104)	0.1171	(54)	0.1242	(52)
	Biso	0.47	(4)	0.9	(2)	0.4	(2)	0.9	(3)	0.4	(3)	0.3	(2)	0.1	(2)
Mg3	x	0.3333		0.3333		0.3333		0.3333		0.3333		0.3333		0.3333	
	y	0.6667		0.6667		0.6667		0.6667		0.6667		0.6667		0.6667	
	z	0.1082	(6)	0.1256	(84)	0.1101	(59)	0.1209	(116)	0.1109	(126)	0.1114	(51)	0.1127	(53)
	Biso	0.29	(6)	0.7	(4)	0.0	(4)	0.6	(5)	0.9	(6)	0.0		0.0	(3)
O1	x	0.2058	(4)	0.2071	(31)	0.2045	(40)	0.1988	(36)	0.2021	(47)	0.2123	(40)	0.2065	(28)
	y	0.0307	(7)	0.0280	(31)	0.0299	(47)	0.0291	(37)	0.0196	(47)	0.0360	(46)	0.0272	(25)
	z	-0.0197	(8)	-0.0211	(100)	-0.0171	(60)	-0.0317	(104)	-0.0328	(126)	-0.0195	(65)	-0.0204	(81)
	Biso	0.03	(7)	0.3	(4)	0.0		0.0		0.0		0.0		0.0	
O2	x	0.4756	(7)	0.4739	(31)	0.4807	(43)	0.4727	(39)	0.4772	(53)	0.4648	(45)	0.4730	(28)
	y	0.0980	(7)	0.0994	(35)	0.0988	(46)	0.1022	(39)	0.0951	(57)	0.1037	(39)	0.1008	(29)
	z	0.4861	(6)	0.4955	(97)	0.4874	(67)	0.4757	(114)	0.5006	(135)	0.4827	(66)	0.4824	(81)
	Biso	0.12	(7)	0.1	(4)	0.0		0.0		0.0		0.0		0.0	
O3	x	0.4515	(6)	0.4533	(33)	0.4505	(39)	0.4528	(38)	0.4463	(45)	0.4511	(39)	0.4497	(27)
	y	0.2925	(6)	0.2868	(38)	0.2881	(43)	0.2880	(41)	0.2875	(49)	0.2832	(37)	0.2863	(28)
	z	0.2360	(6)	0.2750	(75)	0.2308	(60)	0.2564	(111)	0.2117	(149)	0.2427	(68)	0.2552	(71)
	Biso	0.11	(7)	0.0		0.0		0.0		0.0		0.0		0.1	(4)
O4	x	0.1646	(6)	0.1613	(37)	0.1665	(33)	0.1612	(35)	0.1599	(40)	0.1586	(31)	0.1583	(26)
	y	0.4343	(6)	0.4341	(35)	0.4317	(39)	0.4352	(35)	0.4420	(43)	0.4330	(40)	0.4349	(25)
	z	0.2418	(7)	0.2687	(95)	0.2475	(65)	0.2495	(113)	0.2006	(132)	0.2466	(73)	0.2572	(89)
	Biso	0.23	(8)	0.8	(5)	0.0		0.0		0.0		0.1	(5)	0.0	
O5	x	0.6667		0.6667		0.6667		0.6667		0.6667		0.6667		0.6667	
	y	0.3333		0.3333		0.3333		0.3333		0.3333		0.3333		0.3333	
	z	0		0		0		0		0		0		0	
	Biso	0.15	(12)	0.3	(7)	0.4	(8)	0.5	(8)	0.0		0.0		0.0	(6)
O6	x	0		0		0		0		0		0		0	
	y	0		0		0		0		0		0		0	
	z	0.2357	(12)	0.2459	(135)	0.2398	(120)	0.2344	(113)	0.1917	(235)	0.2365	(62)	0.2302	(114)
	Biso	0.00	(12)	1.2	(7)	1	(9)	0.8	(8)	0.4	(9)	0.8	(8)	1.6	(8)

* Results of 2nd run using the same sample with another orientation in DAC.

Table 4. Selected bond distances (Å) of phase A at each pressure condtions

Pressure (GPa)	0	3.6	4.4*	6.2	9.1	9.4*	10.8
Tetrahedron							
Si1-O3 [x3]	1.649 (5)	1.70 (3)	1.59 (5)	1.62 (4)	1.6 (1)	1.59 (4)	1.65 (3)
Si1-O5	1.713 (10)	1.83 (9)	1.75 (10)	1.82 (10)	1.6 (2)	1.72 (9)	1.82 (9)
Mean Si1-O	1.665 (6)	1.73 (5)	1.63 (7)	1.67 (5)	1.6 (2)	1.62 (5)	1.69 (5)
Si2-O1 [x3]	1.670 (6)	1.60 (3)	1.64 (4)	1.51 (3)	1.8 (1)	1.66 (4)	1.61 (4)
Si2-O6	1.632 (10)	1.74 (10)	1.61 (10)	1.74 (10)	1.6 (3)	1.58 (10)	1.70 (10)
Mean Si2-O	1.653 (7)	1.64 (5)	1.63 (6)	1.57 (5)	1.8 (1)	1.64 (6)	1.63 (6)
Octahedron							
M1-O1	1.990 (6)	1.91 (3)	1.97 (4)	1.96 (5)	2.1 (1)	1.94 (3)	1.92 (4)
M1-O2	1.987 (7)	1.94 (3)	1.93 (4)	1.98 (4)	2.2 (1)	1.99 (4)	1.91 (4)
M1-O3	2.241 (7)	2.13 (4)	2.28 (5)	2.07 (6)	2.1 (1)	2.18 (4)	2.05 (5)
M1-O4	2.105 (7)	2.05 (5)	2.05 (5)	2.00 (5)	2.2 (1)	2.06 (4)	2.03 (5)
M1-O4'	2.388 (7)	2.29 (5)	2.36 (5)	2.26 (5)	2.3 (1)	2.25 (4)	2.22 (5)
M1-O5	2.109 (6)	2.01 (4)	2.07 (4)	2.11 (6)	2.2 (1)	2.06 (4)	2.03 (5)
Mean M1-O	2.136 (7)	2.06 (4)	2.11 (5)	2.06 (5)	2.2 (1)	2.08 (4)	2.03 (5)
M2-O1	2.069 (7)	2.20 (5)	2.02 (5)	2.08 (6)	2.1 (1)	2.02 (5)	2.11 (5)
M2-O1'	2.209 (7)	2.28 (5)	2.14 (5)	2.18 (6)	2.1 (1)	2.16 (4)	2.15 (5)
M2-O2	2.032 (7)	2.05 (4)	2.02 (5)	1.98 (5)	1.9 (1)	1.95 (4)	2.03 (4)
M2-O3	2.000 (7)	2.11 (4)	1.97 (4)	2.15 (7)	1.8 (1)	2.03 (4)	2.11 (5)
M2-O4	2.144 (7)	2.14 (4)	2.12 (4)	2.18 (5)	2.0 (1)	2.10 (4)	2.12 (5)
M2-O6	2.168 (6)	2.11 (5)	2.16 (7)	2.18 (7)	1.9 (1)	2.09 (4)	2.03 (5)
Mean M2-O	2.103 (7)	2.15 (5)	2.07 (5)	2.13 (6)	2.0 (1)	2.06 (4)	2.09 (5)
M3-O2 [x3]	2.065 (7)	2.09 (4)	2.03 (5)	2.15 (5)	2.0 (1)	2.05 (4)	2.05 (4)
M3-O4 [x3]	2.075 (7)	2.12 (6)	2.08 (5)	2.01 (6)	1.8 (1)	2.05 (5)	2.09 (6)
Mean M3-O	2.070 (7)	2.11 (5)	2.06 (5)	2.08 (6)	1.9 (1)	2.05 (5)	2.07 (5)

*Results of 2nd run using the same sample with another orientation in DAC.

1975). All X-ray diffraction measurement was performed using an automated four-circle X-ray diffractometer (Rigaku, AFC-7S) with graphite monochromatised MoK α radiation (λ=0,71069 Å, 50 kV 40 mA). The cell parameters of phase A under each pressure condition were determined by 18-25 centered reflections in the 2θ range between 10° and 29°. Refined cell parameters are listed in Table 1. Crystal structures of phase A under high-pressure conditions were refined at ambient pressure, 3.6, 4.4, 6.2, 9.1, 9.4 and 10.8 GPa. The X-ray diffraction intensities of phase A were measured up to $\sin\theta<0.7$ by 2θ-ω scan with fixed ϕ method. The reflection data with $Io>1.5\sigma(Io)$ were used for structure refinements at each pressure point. After Lorentz-polarization corrections, the intensities of symmetrically equivalent reflections were averaged in the Laue group of 6/m. No crystal absorption correction was applied because of the small μ value (μ=8.72 cm^{-1}) and the size of crystal. The initial parameters of phase A with space group $P6_3$ were from Horiuchi et al. (1979). The value of $1/\sigma^2$ was used as weight for structure analysis at ambient pressure. The unit weight was used for the other analyses under high-pressure conditions. All calculations were performed using the teXsan crystallographic software package of Molecular Structure Corporation (1992). The conditions of structure refinements are summarized in Table 2. Final atomic coordinates and the selected bond distances of phase A at each pressure are given in Tables 3 and 4. The observed and calculated structure factors for phase A at each pressure point are given in Appendixes 1-7.

Results and discussion

Although the pressure medium of 4:1 fluid mixture of methanol and ethanol is considered to change a vitreous state under pressure higher than 10 GPa, no anomalous broadening of the ruby fluorescence peaks or the X-ray diffraction peaks from the sample were observed up to 11.2 GPa. We assumed that the specimen was approximately under hydrostatic condition in the pressure range

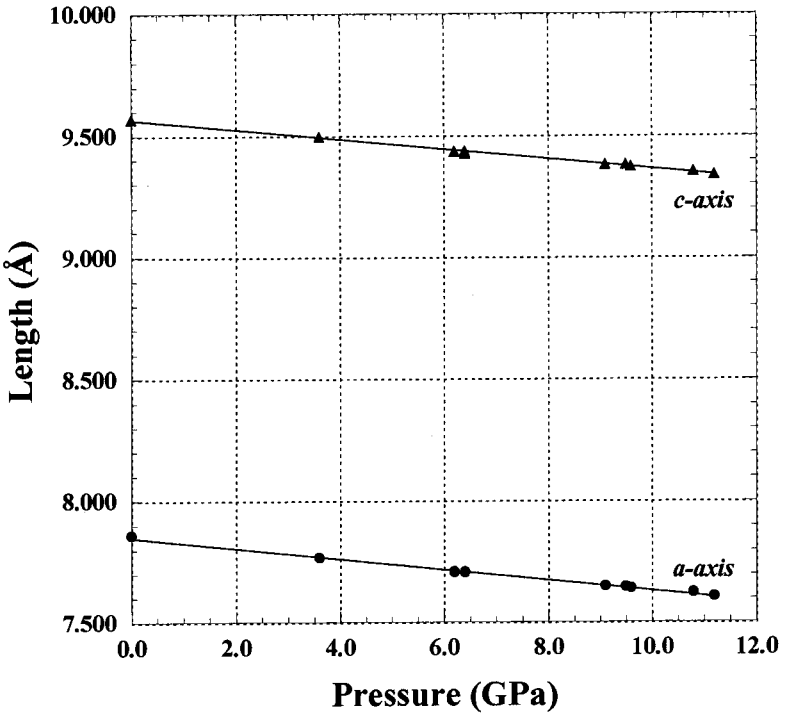

Figure 1. Variation of each axial length of phase A with increasing pressure up to 11.2 GPa.

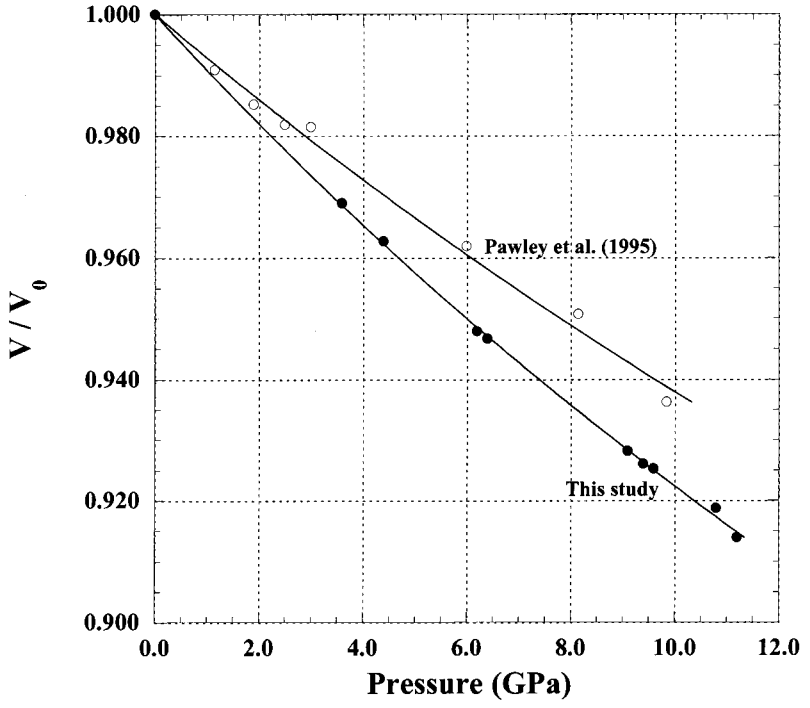

Figure 2. Compression curve of phase A up to 11.2 GPa.

up to 11.2 GPa.

Figure 1 shows a plot of each axial length of phase A with increasing pressure up to 11.2 GPa. Each axial length gradually decreased over this pressure range. The axial linear compressibilities of phase A, which we determined, are β_a=2.92(2) and β_c=2.17(3) ($\times 10^{-3}$/GPa). The *c*-axis, which is perpendicular to the oxygen packing layer of phase A, was less compressible than the [100] direction. Ross and Crichton (2002) performed high-pressure single crystal X-ray diffraction experiment using a DAC up to 7.6 GPa and reported axial compressibility and isothermal bulk modulus. Our results are in good agree-

ment with those of Crichton and Ross (2002), β_a=3.00(5) and β_c=2.30(4) ($\times 10^{-3}$/GPa). Compared to other minerals on the forsterite-brucite join such as OH-chondrodite and OH-clinohumite (the packing direction of oxygen is [100] in both minerals and compression data are from Ross and Crichton, 2001), the linear compressibility of the packing direction of phase A (β_c=0.00217(3)/GPa) was greater than that of OH-chondrodite (β_a=0.00188(3)/GPa) and OH-clinohumite (β_a=0.00175(2)/GPa). In contrast, the linear compressibility of [100] direction of phase A (β_a=0.00292(2)/GPa) is slightly higher than those of OH-chondrodite (β_b=0.00280(3)/GPa and β_c=0.00279(3)/GPa) and is nearly the same as that of OH-clinohumite (β_b=0.00290(4)/GPa). The β_c value (0.00258(3)/GPa) of OH-clinohumite is less than the β_a value of phase A. The compression process of phase A is different from those of humite minerals.

Figure 2 shows the compression curve of phase A up to 11.2 GPa. The isothermal bulk modulus of phase A, calculated from the Birch-Murnaghan equation of state, was 105(4) GPa with a pressure derivative K'= 3.9(8) and V_0=512.2(6) Å^3. This value is consistent with that of Crichton and Ross (2002) (K_{T0}=97.5(4) GPa with K'=5.97(14)), but significantly smaller than that of Pawley et al. (1995) (K_{T0}=145(5) GPa assuming K'=4). Our K' value is significantly lower than that of Crichton and Ross (2002). But both values are within three times the estimated standard deviation. A 4 : 1 fluid mixture of methanol and ethanol was used as a pressure medium in both studies, but Crichton and Ross (2002) determined pressure using the equation of state for quartz (Angel et al., 1997), while we used the ruby fluorescence method (Piermarini et al., 1975). In high-pressure single crystal X-ray diffraction experiments, it is well known that the use of the unit cell parameters determined outside the pressure cell biases the results because of the restriction of the measurable area in a reciprocal space. These affected the calculations for the K_{T0} and K' values. Moreover, because the K' value reflects the initial compression of material, the data around the lower pressure points, especially at ambient pressure, are important. In our study, the estimated standard deviation for K' is higher than that of Crichton and Ross (2002) because of the lack of lower pressure data (under 3 GPa) and the probability of non-hydrostatic conditions in a DAC over 10 GPa. On the other hand, Pawley et al. (1995) carried out high-pressure powder X-ray diffraction study with a DAC up to 10 GPa using a non-dried 4:1 methanol and ethanol mixture as a

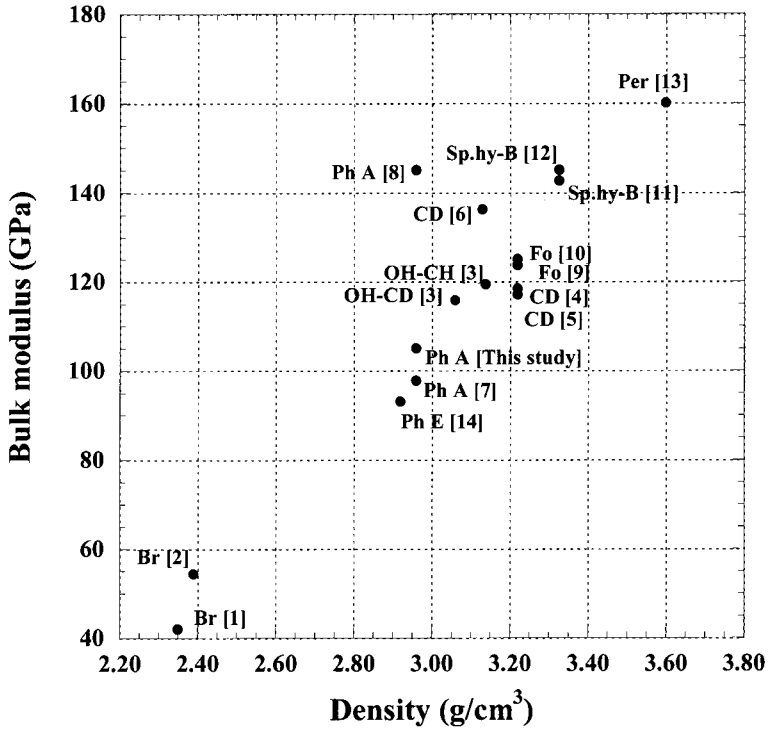

Figure 3. Density versus bulk modulus plots of dense hydrous magnesium silicate and hydroxide in the system MSH. Br, brucite; Ph E, phase E; Ph A, phase A; OH-CD, OH-chondrodite; OH-CH, OH-clinohumite; CD, chondrodite; Fo, forsterite; sp.hy-B, super hydrous phase B; Per, periclase. Compression data from [1] Duffy et al. (1991), [2] Fei and Mao (1993), [3] Ross and Crichton (2002), [4] Sinogeikin and Bass (1999), [5] Friedrich et al. (2002), [6] Faust and Knittle (1994), [7] Crichton and Ross (2002), [8] Pawley et al. (1995), [9] Kudoh and Takeuchi (1985), [10] Downs et al. (1995), [11] Crichton et al. (1999), [12] Kudoh et al. (1995), [13] Fei (1999) and [14] Shieh et al. (2000)

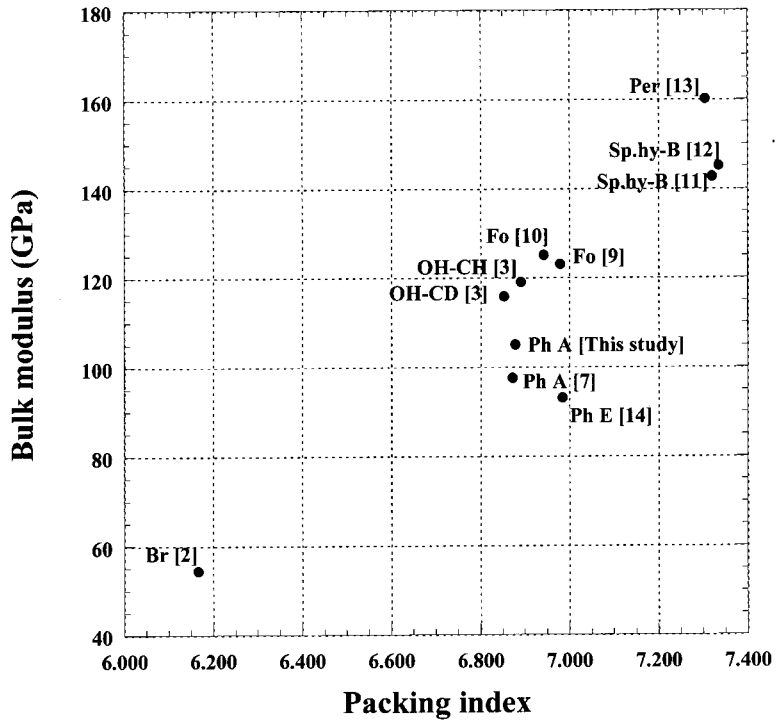

Figure 4. Packing index versus bulk modulus plots of minerals on the forsterite-brucite join in the system MSH. Abbreviations and reference numbers are given in Figure 3.

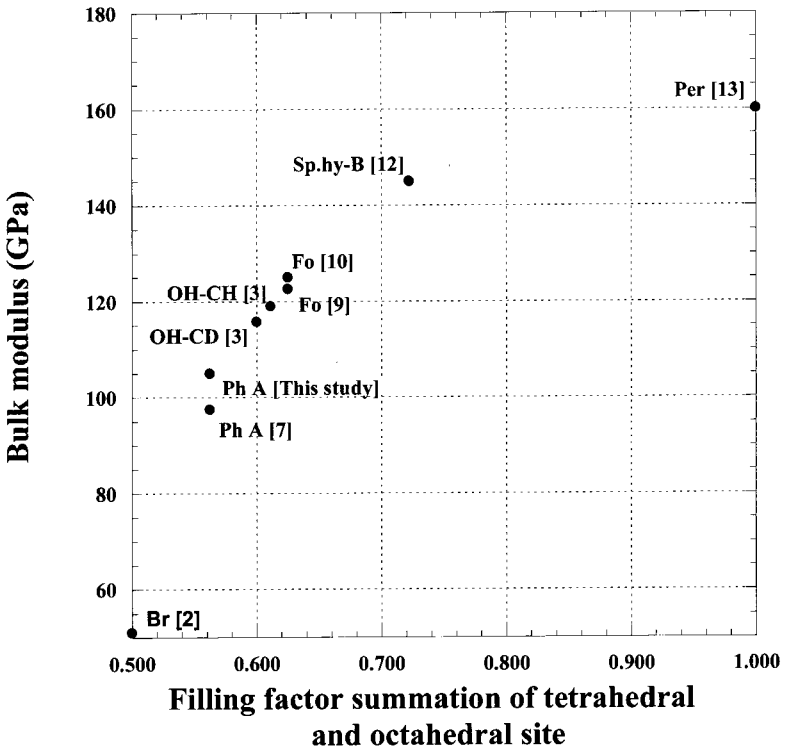

Figure 5. Summation of the filling factor of tetrahedral site and octahedral site versus bulk modulus plots of minerals on the forsterite-brucite join in the system MSH. Abbreviations and reference numbers are given in Figure 3.

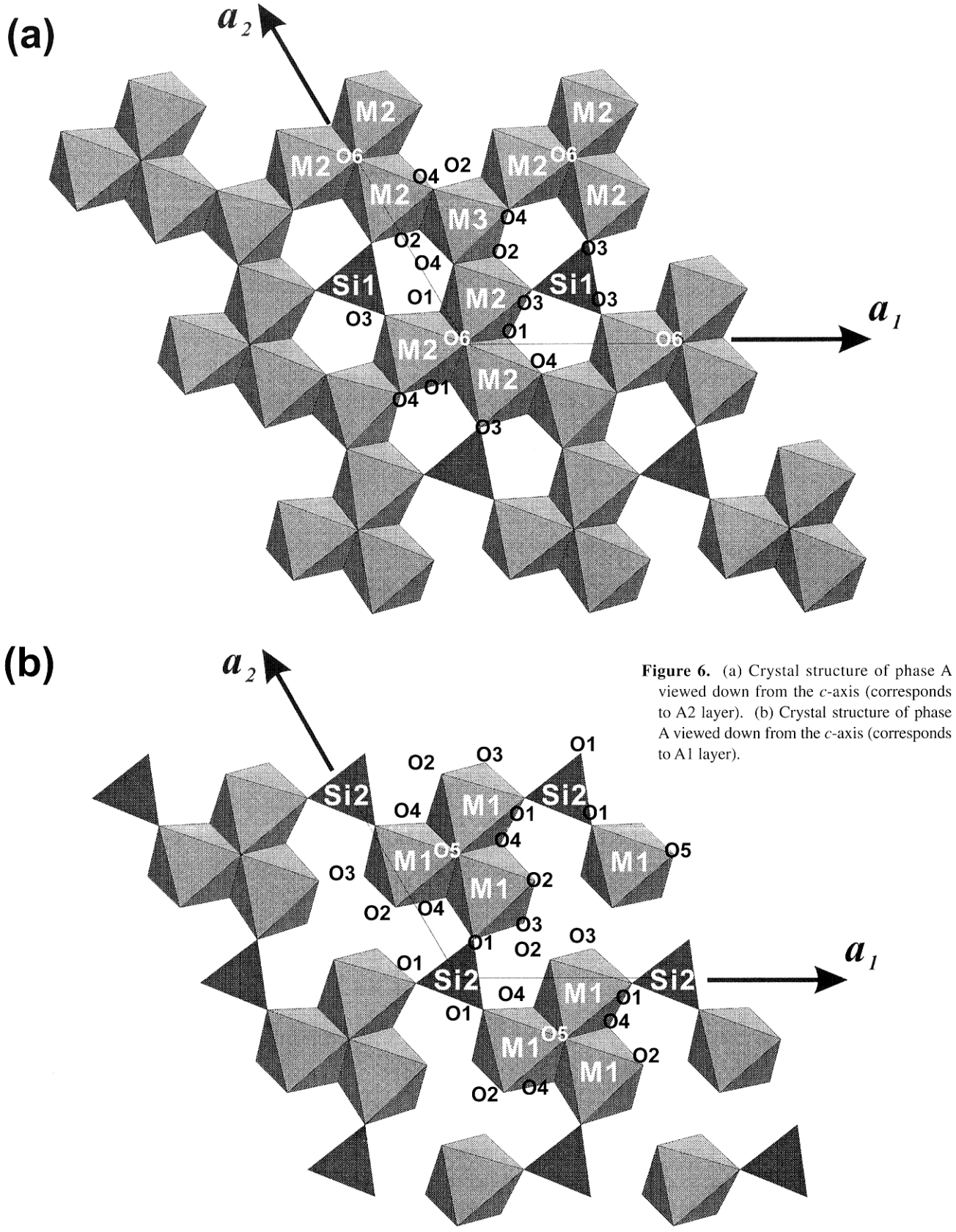

Figure 6. (a) Crystal structure of phase A viewed down from the *c*-axis (corresponds to A2 layer). (b) Crystal structure of phase A viewed down from the *c*-axis (corresponds to A1 layer).

pressure transmitting fluid and NaCl powder as an internal pressure standard. Although a 4 : 1 methanol and ethanol pressure medium is known to be hydrostatic to at least 10 GPa, the phase A powder in a DAC, which Pawley et al. (1995) used, would not be in hydrostatic condition because of insufficient pressure transmitting fluid. Frost and Fei (1999) reported that non-hydrostatic conditions would be generated in high-pressure X-ray powder diffraction experiments. The high-pressure results of Pawley et al. (1995) suggested the experimental conditions were not under hydrostatic condition.

Parise et al. (1998) showed simple correlations between bulk modulus (K) and density (ρ) for dense hydrous magnesium silicate minerals and hydroxides (Fig. 3). Our results are consistent with that trend. However, a plot of packing index versus bulk modulus (Fig. 4) shows another trend. The packing index (Berry and Mason, 1959) is defined as the percentage of the total volume of substance occupied by atoms/ion. This concept assumes that ions behave like spheres supporting each other in a crystal structure and, even with the same numbers of ions, different modes of packing having with different volume requirements, are possible. We assumed the ionic radius of Mg, Si, and O as 0.8, 0.3 and 1.4 (Å), respectively. It is derived from crystal structure data in the following way: packing index (P.I.) = (volume of ions / volume of unit cell)×10. Forsterite and humite minerals fall on one trend but phase A does not. Figure 4 shows that although the packing index of phase A has the nearly same value as those of humite minerals, the bulk modulus of phase A is significantly smaller. Other dense hydrous magnesium silicate minerals show the same trend as that of phase A. This suggests that the compression mechanism for phase A is different from that of humite minerals.

In all structures of forsterite, humite minerals and phase A, one half of the octahedral sites are occupied, but the occupancies of the tetrahedral site for these minerals are different (1/8 for forsterite, 1/10 for chondrodite, 1/9 for clinohumite and 1/16 for phase A). The filling factor for polyhedral (tetrahedral and octahedral) sites is defined as the ratio of (the occupied polyhedral site) / (the total number of each polyhedral site) in its structure. A plot of bulk modulus versus the summation of filling factor for tetrahedral and octahedral sites shows a good correlation for humite minerals but not for phase A (Fig. 5). This indicates that the tetrahedral site should affect the compression mechanism of these minerals. In humite minerals, the crystal structure consists of a slightly distorted ABAB type hexagonal closest packing. The replacements of $Si^{4+}+4O^{2-} \leftrightarrow \square + 4(OH, F)^-$ are generated in humite homologous series, which are described as $Mg_{2x}Si_{x-1}O_{4x-4}(OH, F)_4$ (x=3,5,7, and 9). In contrast, the crystal structure of phase A is composed of an ABCB type closest packed anion array, forming two type layers, A1 and A2, which are stacked alternately along the c-axis (Fig. 6a, b). The crystal structure of phase A has the characteristic octahedral vacancy site. Kudoh et al, (2002) described A1 and A2 layers. The A2-layer is composed of $Si1O_4$ tetrahedra, $Mg2O_6$ and $Mg3O_6$ octahedra. The $Mg2O_6$ octahedron shares edges with other symmetrically equivalent $Mg2O_6$ octahedra to form $Mg2_3O_{13}$ group. This group is linked to others by sharing edges with $Mg3O_6$ octahedron. The $Mg2O_6$ octahedron is the same type of octahedron found in forsterite and humite minerals. The $Si1O_4$ tetrahedron shares corners with $Mg2O_6$ octahedra. The $Si1O_4$ tetrahedron shares no edge with octahedra. In contrast, the A1-layer is composed of $Si2O_4$ tetrahedra and $Mg1O_6$ octahedra. The $Mg1O_6$ octahedron forms $Mg1_3O_{13}$ group like $Mg2O_6$ octahedron in the A2-layer. Although these groups are isolated, they are linked to others by sharing the corners with $Si2O_4$ tetrahedra (Horiuchi et al. 1979). While the crystal structures of humite minerals consist of only one type layer for each mineral, the A1- and A2- layers in the phase A structure are connected by two types of tetrahedra. The layers in humite minerals are connected by only one type of tetrahedron similar to the $Si2O_4$ tetrahedron in phase A. The structure analyses of phase A under high-pressure conditions showed that the mean Si1-O and Si2-O bond distances in each tetrahedron remain almost unchanged, 1.662(6) Å → 1.69(5) Å and 1.653(7) Å → 1.64(6) Å, respectively. This shows that the tetrahedron should behave like a rigid body in this pressure range. In contrast, for octahedral sites, the decreasing ratios of the mean M-O distance in each octahedron up to 10.8 GPa are 0.95 for $Mg1O_6$, 0.99 for $Mg2O_6$ and 1.00 for $Mg3O_6$. The mean M-O distance of $Mg1O_6$ octahedron, which forms isolated $Mg1_3O_{13}$ block, is most compressible. This octahedron is the characteristic octahedron in the phase A structure compared with the crystal structures of humite minerals. The total void space volume is calculated from the deficit of the summation of all the polyhedral volume from the unit cell volume. The bulk modulus of total vacancy space in phase A, calculated from the Birch-Murnaghan equation of state, is $K_\square$=97(2) GPa, assuming K_{T0}'=4. This result shows that the void space of phase A is more compressible than the occupied octahedral site in the phase A structure. The characteristic large void space, which is present in the phase A structure, corresponds to the octahedral vacancy site. This site would control its compression. The oxygen sites related to this octahedral vacancy site in the phase A structure are O2 and O3. Over the same pressure range, the O2-O3 distance (2.900(7) and 2.897(7) Å at ambient condition → 2.69(8) and 2.61(8) Å at 10.8 GPa), which

corresponds to compression in the stacking direction, decreases more than the O3-O4 distance (3.092(8) Å at ambient condition → 2.99(3) Å at 10.8 GPa), which corresponds to horizontal compression. Kagi et al. (2000) reported the deuterium positions in phase A structure using powder neutron diffraction. They reported that hydrogen is located near the octahedral vacancy site and forms two types of hydrogen bonding, which they described as O2-H···O3 and O4-H···O3. Kudoh et al. (2001) reported that the O2-O3 bond distances decreased about 10% more than the O4-O3 bond distance (6%) under pressures up to 9.4 GPa. Our result is consistent with that of Kudoh et al. (2001). The characteristic compression of this vacancy site should be influenced by the strength of the hydrogen bonding.

The differences of the compression mechanisms between phase A and humite minerals are shown using the packing index and the filling factor. These parameters may be useful to understand the effects of pressure for homologous series minerals. It is especially useful to clarify the effects of the replacements between OH and F on the pressure behavior in humite minerals. The detailed compression mechanism was significantly different between phase A and humite minerals. However, crystal structure data of humite minerals under high-pressure condition is lacking. Further data on the crystal structure of humite minerals under high-pressure conditions is needed in order to confirm the differences in the compression mechanism between phase A and humite minerals.

Acknowledgements

The authors are grateful to Professor Nakazawa for helpful comments and discussion about systematic considerations on humite minerals and phase A. Helpful comments from two anonymous reviewers are also appreciated.

References

Angel, R. J., Allan, D.R., Miletich, R. and Finger, L. W. (1997) The use of quartz as an internal pressure standard in high-pressure crystallography. Journal of Applied Crystallography, 30, 461-466.

Bass, J. D., Kanzaki, M. and Howell, D. A. (1991) Sound velocities and elastic properties of phase E: a high pressure hydrous silicate. EOS transactions of American Geophysical Union, 72, 499.

Berry, L. G. and Mason, B. (1959) Mineralogy. Concepts, Description, Determinations. p137, San Franscisco, W. H. Freeman and Company.

Burnley, P. C. and Navrotsky, A. (1996) Synthesis of high-pressure hydrous magnesium silicates: Observations and Analysis. American Mineralogist, 81, 317-326.

Crichton, W. A. and Ross, N. L. (2002) Equation of state of dense hydrous magnesium silicate phase A, $Mg_7Si_2O_8(OH)_6$. American Mineralogist, 87, 333-338.

Crichton, W. A., Ross, N. L. and Gasparik, T. (1999) Equation of state of magnesiu, silicates anhydrous B and super hydrous B. Physics and Chemistry of Minerals, 26, 570-575

Downs, R. T., Zha, C.-S., Duffy, T. S. and Finger, L. W. (1996) The equation state of forsterite to 17.2 GPa and effects of pressure media. American Mineralogist, 81, 51-55.

Duffy, T. S., Ahrens, T. J. and Lange, M. A. (1991) The shock wave equation of state of brucite $Mg(OH)_2$. Journal of Geophysical Research, 96, 14319-14330.

Faust, J. and Knittle, E. (1994) Static compression of chondrodite: Implications for water in the upper mantle. Geophysical Research Letters, 21, 1935-1938.

Fei, Y. (1999) Effects of temperature and composition on the bulk modulus of (Mg, Fe)O. American Mineralogist, 84, 272-276

Fei, Y. and Mao, Ho-k. (1993) Static compression of $Mg(OH)_2$ to 78 GPa at high temperature and constraints on the equation state of fluid H_2O. Journal of Geophysical Research, 98, 11875-11884.

Friedrich, A., Lager, G. A., Ulmer, P. Kunz, M. and Marshall, W. G. (2002) High-pressure single-crystal X-ray and powder neutron study of F,OH/OD-chondrodite: Compressibility, structure, and hydrogen bonding. American Mineralogist, 87, 931-939.

Frost, D. J. and Fei, Y. (1999) Static compression of the hydrous magnesium silicate phase D to 30 GPa at room temperature. Physics and Chemistry of Minerals, 26, 415-418.

Horiuchi, H., Morimoto, N., Yamamoto, K. and Akimoto, S. (1979) Crystal structure of $2Mg_2SiO_4{\cdot}3Mg(OH)_2$, a new high-pressure structure type. American Mineralogist, 64, 593-598.

Kagi, H., Parise, J. B., Cho, H. M., Rossman, G. R. and Loveday, J. S. (2000) Hydrogen bonding interaction in phase A [$Mg_7Si_2H_6O_{14}$] at ambient and high pressure. Physics and Chemistry of Minerals, 27, 225-233.

Kanzaki (1991) Stability of hydrous magnesium silicates in the mantle transition zone. Physics of the Earth and Planetary Interiors, 66, 307-312.

Kudoh, Y. and Takeuchi, Y. (1985) The crystal structure of forsterite Mg_2SiO_4 under high pressure up to 14.9 GPa. Zeutschrift für Kristallographie, 171, 291-302.

Kudoh, Y. and Takeda, H. (1986) Single crystal X-ray diffraction study on the bond compressibility of fayalite, Fe_2SiO_4 and rutile, TiO_2 under high-pressure. Physica, 139&140B, 333-336.

Kudoh, Y., Kuribayashi, T., Kagi, H., Sasaki, S. and Tanaka, M. (2002) High-pressure structural study of phase-A, $Mg_7Si_2H_6O_{14}$ using synchrotron radiation. Journal of Physics: Condensed Matter, 14, 10491-10495.

Kuribayashi, T., Kudoh, Y. and Kagi, H. (1999) High-pressure X-ray diffraction study on phase A, $Mg_7Si_2H_6O_{14}$, up to 11.2 GPa. EOS transactions of the American Geophysical Union, 80, F938.

Parise, J. B., Cox, H., Kagi, H., Li, R., Marshall, W. G., Loveday, J. S. and Klotz, S. (1998) Hydrogen bonding in $M(OD)_2$ compounds under pressure. In the Review of High Pressure Science and Technology (Nakahara, M. Ed.). Proceedings of International Conference-AIRAPT-16 and HPCJ-38- on high pressure Science and Technology, 7, 211-216.

Pawley, A. R. (2000) Stability of clinohumite in the system MgO-SiO_2-H_2O. Contribution to Mineralogy and Petrology, 138,

284-291.

Pawley, A. R., Redfern, S. A. T. and Wood, B. J. (1995) Thermal expansivities and compressibilities of hydrous phases in the system MgO-SiO_2-H_2O: talc, phase A and 10Å phase. Contribution to Mineralogy and Petrology, 122, 301-307.

Piermarini, G. V., Block, S., Bernett, J. and Forman, R. A. (1975) Calibration of the pressure dependence of the R1 ruby fluorescence line to 195 kbar. Journal of Applied physics, 46, 2774-2780.

Ringwood, A. E. and Major, A. (1967) High-pressure reconnaissance investigations in system Mg_2SiO_4-MgO-H_2O. Earth and Planetary Science Letters, 2, 130-133.

Ross, N. L. and Crichton, W. A. (2001) Compression of hydroxylclinohumite, $[Mg_9Si_4O_{16}(OH)_2]$ and hydroxylchondrodite, $[Mg_5Si_2O_8(OH)_2]$. American Mineralogist, 86, 990-996.

Shieh, S. R., Mao, Ho-k, Konzett, J. and Hemley, R. J. (2000) In situ high pressure X-ray diffraction of phase E to 15 Gpa. American Mineralogist, 85, 765-769.

Sinogeikin, S. V. and Bass, J. D. (1999) Single-crystal elastic properties of chondrodite: Implications for water in the upper mantle. Physics and Chemistry of Minerals, 26, 297-303.

teXsan (1992) Crystal Structure Analysis Package, Molecular Structure Corporation, Texas, USA.

Ulmer, P. and Trommsdorf, V. (1995) Serpentine stability to mantle depths and subduction-related magmatism. Science, 268, 858-861.

Wunder, B. (1998) Equilibrium experiments in the system MgO-SiO_2-H_2O (MSH): stability fields of clinohumite-OH $[Mg_9Si_4O_{16}(OH)_2]$, chondrodite-OH $[Mg_5Si_2O_8(OH)_2]$ and phase A $[Mg_7Si_2O_8(OH)_6]$. Contribution to Mineralogy and Petrology, 132, 111-120.

Yamamoto, K. and Akimoto, S. (1974) High pressure and high temperature investigation in the system MgO-SiO_2-H_2O. Journal of Solid State Chemistry, 9, 187-195.

Yamamoto, K. and Akimoto, S. (1977) The system MgO-SiO_2-H_2O at high pressure and temperatures – stability fields for hydroxyl-chondrodite, hydroxyl-clinohumite and 10Å-phase. American Journal of Science, 277, 288-312.

Manuscript received, 3 October, 2003
Manuscript accepted, 26 December, 2003

Appendix 1. The observed and calculated structure factor for phase A at ambient condition data

h	*k*	*l*	*Fo*	*Fc*	*h*	*k*	*l*	*Fo*	*Fc*	*h*	*k*	*l*	*Fo*	*Fc*	*h*	*k*	*l*	*Fo*	*Fc*	*h*	*k*	*l*	*Fo*	*Fc*
0	0	2	209	202	1	2	6	447	450	1	5	10	87	54	2	0	11	74	74	2	4	0	172	169
0	0	4	884	875	1	2	7	159	141	1	6	0	63	10 *	2	0	12	246	250	2	4	1	88	87
0	0	6	536	497	1	2	8	267	268	1	6	1	86	123	2	0	13	43	74 *	2	4	2	271	273
0	0	8	1180	1120	1	2	9	0	38 *	1	6	2	388	403	2	1	0	55	59	2	4	3	94	108
0	0	10	552	484	1	2	10	0	99 *	1	6	3	188	201	2	1	1	40	32 *	2	4	4	0	52 *
0	0	12	354	365	1	2	11	135	118	1	6	4	101	117	2	1	2	1142	1107	2	4	5	185	179
					1	2	12	270	258	1	6	5	315	328	2	1	3	978	939	2	4	6	51	25 *
1	0	0	115	102	1	3	0	58	23 *	1	6	6	112	116	2	1	4	717	665	2	4	7	218	227
1	0	1	55	82	1	3	1	215	200	1	6	7	77	114 *	2	1	5	1290	1238	2	4	8	77	114 *
1	0	2	205	189	1	3	2	111	123	1	6	8	57	99 *	2	1	6	715	692	2	4	9	134	129
1	0	3	348	364	1	3	3	340	360	1	6	9	164	147	2	1	7	77	116	2	4	10	0	10 *
1	0	4	120	112	1	3	4	140	131	1	7	0	345	354	2	1	8	51	52 *	2	4	11	0	34 *
1	0	5	148	145	1	3	5	98	118	1	7	1	44	50 *	2	1	9	531	495	2	5	0	258	259
1	0	6	258	264	1	3	6	262	259	1	7	2	70	98 *	2	1	10	485	478	2	5	1	313	324
1	0	7	378	399	1	3	7	355	381	1	7	3	49	63 *	2	1	11	267	273	2	5	2	106	109
1	0	8	35	58 *	1	3	8	0	26 *	1	7	4	373	355	2	1	12	301	281	2	5	3	315	330
1	0	9	64	61	1	3	9	81	60	1	7	5	63	78 *	2	2	0	167	173	2	5	4	255	261
1	0	10	150	151	1	3	10	222	227	1	7	6	71	57 *	2	2	1	237	242	2	5	5	155	148
1	0	11	97	123	1	3	11	188	179	1	7	7	0	32 *	2	2	2	134	141	2	5	6	62	64 *
1	0	12	50	72 *	1	3	12	44	28 *	1	7	8	129	117	2	2	3	190	211	2	5	7	362	345
1	0	13	63	18 *	1	4	0	2005	2024	1	8	0	130	151	2	2	4	179	192	2	5	8	0	65 *
1	1	0	467	455	1	4	1	0	10 *	1	8	1	122	119	2	2	5	0	14 *	2	5	9	0	59 *
1	1	1	397	430	1	4	2	115	103	1	8	2	154	186	2	2	6	131	121	2	5	10	57	20 *
1	1	2	165	180	1	4	3	33	4 *	1	8	3	218	221	2	2	7	108	134	2	6	0	126	118
1	1	3	465	481	1	4	4	493	475	1	8	4	0	76 *	2	2	8	223	218	2	6	1	97	119
1	1	4	193	214	1	4	5	25	3 *	1	8	5	35	31 *	2	2	9	14	64 *	2	6	2	349	360
1	1	5	192	188	1	4	6	311	299	1	8	6	234	246	2	2	10	113	118	2	6	3	148	159
1	1	6	84	76	1	4	7	0	4 *	1	9	0	46	118 *	2	2	11	131	141	2	6	4	101	114
1	1	7	343	377	1	4	8	723	705	1	9	1	0	10 *	2	2	12	198	180	2	6	5	86	83
1	1	8	160	134	1	4	9	62	5 *						2	3	0	277	266	2	6	6	254	243
1	1	9	76	58	1	4	10	375	341	2	0	0	77	75	2	3	1	241	229	2	6	7	119	117
1	1	10	126	124	1	4	11	0	3 *	2	0	1	230	221	2	3	2	160	154	2	6	8	88	140
1	1	11	246	238	1	5	0	19	51 *	2	0	2	744	762	2	3	3	184	195	2	7	0	0	70 *
1	1	12	196	182	1	5	1	149	140	2	0	3	75	75	2	3	4	31	15 *	2	7	1	148	145
1	1	13	0	24 *	1	5	2	312	301	2	0	4	196	213	2	3	5	217	232	2	7	2	40	82 *
1	2	0	174	170	1	5	3	205	197	2	0	5	256	264	2	3	6	88	86	2	7	3	166	168
1	2	1	258	255	1	5	4	82	82	2	0	6	357	365	2	3	7	382	401	2	7	4	0	39 *
1	2	2	698	717	1	5	5	76	60	2	0	7	136	126	2	3	8	146	134	2	7	5	6	46 *
1	2	3	281	287	1	5	6	0	64 *	2	0	8	230	248	2	3	9	202	206	2	7	6	146	155
1	2	4	204	211	1	5	8	62	35 *	2	0	9	129	116	2	3	10	58	87 *	2	8	0	631	659
1	2	5	141	142	1	5	9	0	23 *	2	0	10	132	126	2	3	11	112	105	2	8	1	0	31 *

* Unobserved refrection.

Appendix 1. (Continued)

h	*k*	*l*	*Fo*	*Fc*	*h*	*k*	*l*	*Fo*	*Fc*	*h*	*k*	*l*	*Fo*	*Fc*	*h*	*k*	*l*	*Fo*	*Fc*	*h*	*k*	*l*	*Fo*	*Fc*
2	8	2	53	35 *	3	3	0	204	194	3	7	0	184	218	4	2	10	343	370	5	0	4	125	111
2	8	3	21	15 *	3	3	1	315	333	3	7	1	203	209	4	2	11	199	199	5	0	5	62	56
					3	3	2	173	168	3	7	2	142	133	4	3	0	89	80	5	0	6	232	235
3	0	0	444	444	3	3	3	301	327	3	7	3	59	50 *	4	3	1	0	42 *	5	0	7	262	255
3	0	1	63	105	3	3	4	163	179	3	7	4	0	5 *	4	3	2	243	258	5	0	8	148	142
3	0	2	205	204	3	3	5	96	116						4	3	3	176	178	5	0	9	0	22 *
3	0	3	235	240	3	3	6	102	109	4	0	0	299	308	4	3	4	100	133	5	0	10	110	125
3	0	4	424	439	3	3	7	280	301	4	0	1	215	214	4	3	5	0	55 *	5	0	11	57	87 *
3	0	5	144	130	3	3	8	137	136	4	0	2	247	261	4	3	6	176	167	5	1	0	49	52 *
3	0	6	33	56 *	3	3	9	112	95	4	0	3	395	415	4	3	7	208	203	5	1	1	203	208
3	0	7	89	111	3	3	10	57	37 *	4	0	4	179	183	4	3	8	142	137	5	1	2	383	396
3	0	8	148	145	3	3	11	180	195	4	0	5	44	59 *	4	3	9	43	76 *	5	1	3	155	163
3	0	9	12	21 *	3	4	0	176	154	4	0	6	381	382	4	3	10	112	80	5	1	4	68	86 *
3	0	10	232	237	3	4	1	130	128	4	0	7	338	355	4	4	0	490	473	5	1	5	331	334
3	0	11	80	116	3	4	2	411	433	4	0	8	196	197	4	4	1	30	47 *	5	1	6	66	85 *
3	0	12	119	145	3	4	3	79	85	4	0	9	0	37 *	4	4	2	175	196	5	1	7	143	151
3	1	0	0	18 *	3	4	4	156	154	4	0	10	292	282	4	4	3	150	145	5	1	8	116	117
3	1	1	170	167	3	4	5	234	229	4	0	11	171	174	4	4	4	425	425	5	1	9	224	204
3	1	2	399	423	3	4	6	244	262	4	0	12	31	56 *	4	4	5	125	142	5	1	10	44	86 *
3	1	3	126	141	3	4	7	32	84 *	4	1	0	505	509	4	4	6	66	98 *	5	2	0	209	201
3	1	4	183	189	3	4	8	155	165	4	1	1	123	121	4	4	7	0	75 *	5	2	1	109	104
3	1	5	123	123	3	4	9	0	65 *	4	1	2	214	221	4	4	8	115	114	5	2	2	0	38 *
3	1	6	170	179	3	4	10	96	88	4	1	3	248	270	4	4	9	60	94 *	5	2	3	0	34 *
3	1	7	187	199	3	5	0	0	29 *	4	1	4	300	285	4	5	0	60	5 *	5	2	4	267	262
3	1	8	151	175	3	5	1	97	66	4	1	5	179	189	4	5	1	113	118	5	2	5	102	91
3	1	9	163	149	3	5	2	281	319	4	1	6	42	49 *	4	5	2	137	146	5	2	6	108	87
3	1	10	115	103	3	5	3	273	294	4	1	7	198	191	4	5	3	32	61 *	5	2	7	104	86
3	1	11	77	81 *	3	5	4	190	202	4	1	8	54	48 *	4	5	4	106	97	5	2	8	169	178
3	1	12	112	126	3	5	5	551	529	4	1	9	0	53 *	4	5	5	179	162	5	2	9	66	34 *
3	2	0	258	238	3	5	6	342	342	4	1	10	199	203	4	5	6	29	56 *	5	2	10	156	158
3	2	1	324	331	3	5	7	74	81 *	4	1	11	87	105	4	5	7	102	127	5	3	0	76	88 *
3	2	2	653	690	3	5	8	34	18 *	4	2	0	153	108	4	6	0	195	194	5	3	1	196	203
3	2	3	137	127	3	5	9	247	224	4	2	1	119	79	4	6	1	184	191	5	3	2	166	181
3	2	4	215	223	3	6	0	72	64 *	4	2	2	508	515	4	6	2	350	346	5	3	3	273	278
3	2	5	195	200	3	6	1	65	77 *	4	2	3	461	463	4	6	3	57	48 *	5	3	4	64	98 *
3	2	6	473	487	3	6	2	36	57 *	4	2	4	388	376	4	6	4	116	132	5	3	5	41	31 *
3	2	7	150	135	3	6	3	26	84 *	4	2	5	799	755	4	6	5	143	144	5	3	6	252	248
3	2	8	270	260	3	6	4	111	121	4	2	6	448	452	5	0	0	263	266	5	3	7	225	215
3	2	9	0	47 *	3	6	5	111	104	4	2	7	108	95	5	0	1	71	99	5	3	8	95	84
3	2	10	96	97	3	6	6	0	78 *	4	2	8	36	35 *	5	0	2	76	109	5	3	9	0	71 *
3	2	11	75	80	3	6	7	39	90 *	4	2	9	343	323	5	0	3	291	307	5	4	0	197	202

* Unobserved refrection.

Appendix 1. (Continued)

h	*k*	*l*	*Fo*	*Fc*		*h*	*k*	*l*	*Fo*	*Fc*		*h*	*k*	*l*	*Fo*	*Fc*	
5	4	1	53	66	*	6	2	4	0	23	*	7	2	0	232	224	
5	4	2	98	108		6	2	5	116	115		7	2	1	198	200	
5	4	3	223	226		6	2	6	118	114		7	2	2	145	157	
5	4	4	90	84		6	2	7	244	266		7	2	3	0	37	*
5	4	5	0	45	*	6	2	8	100	124		7	2	4	0	23	*
5	4	6	212	235		6	3	0	855	878		7	2	5	205	191	
5	4	7	216	224		6	3	1	0	45	*	7	2	6	30	51	*
5	5	0	271	266		6	3	2	62	41	*	7	3	0	0	71	*
5	5	1	0	26	*	6	3	3	43	38	*	7	3	1	136	114	
5	5	2	104	96		6	3	4	274	255		7	3	2	219	233	
5	5	3	94	114		6	3	5	0	29	*	7	3	3	107	92	
5	5	4	128	108		6	3	6	166	136		7	3	4	44	56	*
5	5	5	110	125		6	3	7	33	33	*	7	3	5	28	70	*
5	6	0	0	22	*	6	4	0	77	91	*						
5	6	1	21	72	*	6	4	1	88	92		8	0	0	68	59	*
						6	4	2	208	196		8	0	1	0	55	*
6	0	0	333	344		6	4	3	142	148		8	0	2	98	98	
6	0	1	223	222		6	4	4	99	69		8	0	3	52	91	*
6	0	2	51	100	*	6	4	5	7	45	*	8	0	4	168	168	
6	0	3	234	256		6	5	0	0	37	*	8	0	5	0	26	*
6	0	4	212	208		6	5	1	110	136		8	0	6	87	103	
6	0	5	147	154								8	0	7	171	190	
6	0	6	0	41	*	7	0	0	0	25	*	8	1	0	191	185	
6	0	7	243	258		7	0	1	63	58	*	8	1	1	161	164	
6	0	8	40	44	*	7	0	2	280	304		8	1	2	278	278	
6	0	9	0	7	*	7	0	3	277	301		8	1	3	0	24	*
6	0	10	43	88	*	7	0	4	228	229		8	1	4	111	128	
6	1	0	215	206		7	0	5	560	532		8	1	5	159	172	
6	1	1	263	258		7	0	6	306	322		8	1	6	265	274	
6	1	2	496	517		7	0	7	55	87	*	8	2	0	178	164	
6	1	3	173	178		7	0	8	31	18	*	8	2	1	180	181	
6	1	4	170	178		7	0	9	219	219		8	2	2	97	126	
6	1	5	147	147		7	1	0	141	119		8	2	3	166	173	
6	1	6	379	379		7	1	1	110	114							
6	1	7	101	108		7	1	2	125	126		9	0	0	339	311	
6	1	8	212	193		7	1	3	21	76	*	9	0	1	46	59	*
6	1	9	40	60	*	7	1	4	85	88		9	0	2	146	145	
6	2	0	163	178		7	1	5	0	21	*	9	0	3	49	125	*
6	2	1	83	99		7	1	6	61	70	*	9	0	4	238	232	
6	2	2	101	106		7	1	7	0	75	*	9	1	0	0	31	*
6	2	3	148	141		7	1	8	64	118	*	9	1	1	0	56	*

* Unobserved refrection.

Appendix 2. The observed and calculated structure factos for phase A at 3.6 GPa

h	*k*	*l*	*Fo*	*Fc*	*h*	*k*	*l*	*Fo*	*Fc*	*h*	*k*	*l*	*Fo*	*Fc*
1	0	1	51	67	3	1	1	208	226	6	0	4	191	214
1	1	0	498	420	3	1	3	292	335	6	1	2	364	353
1	1	1	380	415	3	2	0	233	255	6	1	3	158	179
1	1	2	136	166	3	2	1	188	191	6	2	2	279	293
1	2	2	1049	1051	3	2	2	152	117	6	3	3	73	76
1	3	2	377	392	3	3	0	179	182	6	4	0	210	184
1	3	3	141	149	3	3	1	296	278	6	4	1	215	166
1	4	0	437	452	3	3	2	171	151					
1	4	2	180	206	3	3	3	258	284	7	0	2	293	268
1	4	3	252	248	3	5	3	254	233	7	0	3	288	289
1	5	2	405	377	3	6	0	728	768	7	0	4	188	197
1	5	3	131	129	3	6	4	240	233	7	1	0	303	316
1	6	2	471	458	3	7	2	147	191	7	1	4	322	343
1	6	3	183	167						7	2	1	153	144
1	6	4	171	154	4	0	0	283	318					
1	8	0	164	142	4	0	1	197	191	8	0	4	153	147
1	8	2	258	246	4	0	2	230	243	8	1	0	149	156
					4	0	3	362	371	8	1	2	126	158
2	0	1	214	220	4	1	0	1977	1922	8	2	0	506	556
2	0	2	659	720	4	1	2	111	117					
2	1	0	187	182	4	1	4	474	468	9	0	2	159	120
2	1	1	255	259	4	2	2	232	243					
2	1	2	615	653	4	3	1	141	161					
2	2	1	210	240	4	3	2	382	386					
2	2	2	155	159	4	4	0	436	407					
2	2	3	159	176	4	4	4	384	381					
2	3	0	215	225	4	5	3	184	169					
2	3	1	317	340	4	6	2	221	183					
2	3	2	638	653										
2	3	3	136	143	5	0	0	239	226					
2	4	2	502	469	5	0	3	251	256					
2	4	3	485	443	5	1	1	143	130					
2	4	4	398	372	5	1	2	294	284					
2	5	0	201	193	5	1	3	175	166					
2	5	4	265	282	5	2	0	227	241					
2	6	0	175	159	5	2	1	295	281					
2	7	0	214	193	5	2	4	212	224					
2	7	1	164	168	5	3	2	273	286					
2	8	0	171	144	5	3	3	274	276					
2	8	1	140	133	5	4	2	169	154					
3	0	0	443	435	6	0	3	252	249					

Appendix 3. The observed and calculated structure factors for phase A at 4.4 GPa

h	*k*	*l*	*Fo*	*Fc*	*h*	*k*	*l*	*Fo*	*Fc*	*h*	*k*	*l*	*Fo*	*Fc*
1	0	0	110	129	2	7	1	259	202	5	2	1	307	310
1	0	1	67	117						5	2	3	309	311
1	0	2	179	185	3	0	0	428	423	5	3	2	280	307
1	0	3	321	369	3	0	4	392	443	5	3	3	337	289
1	1	0	458	470	3	1	3	319	369	5	3	5	549	543
1	1	1	405	393	3	1	4	171	169	5	3	6	348	351
1	1	2	168	172	3	1	7	369	396					
1	1	3	422	501	3	2	0	233	265	6	0	1	208	215
1	2	2	1188	1066	3	2	1	211	228	6	0	3	284	250
1	2	5	1281	1257	3	2	3	197	215	6	0	4	223	225
1	2	6	692	661	3	3	1	294	312	6	1	2	409	447
1	3	4	183	169	3	3	7	221	271	6	2	2	364	360
1	4	0	440	477	3	5	1	227	183	6	2	6	234	238
1	4	2	214	210	3	5	3	308	280	6	4	1	247	199
1	4	3	266	277	3	5	6	302	265	6	4	2	361	338
1	4	4	333	307	3	6	0	881	896					
1	5	5	280	310	3	6	4	299	271	7	0	2	292	291
1	6	1	260	259						7	0	3	273	297
1	6	2	480	502	4	0	0	293	319	7	0	5	535	547
1	6	6	334	354	4	0	1	176	214	7	0	6	423	329
1	6	8	266	210	4	0	2	243	225	7	1	4	327	384
1	8	2	316	290	4	0	4	187	185	7	2	3	225	173
					4	0	7	315	353	7	3	0	263	215
2	0	1	229	247	4	1	0	1988	2009					
2	0	2	730	776	4	1	4	478	472	8	2	0	665	683
2	1	0	193	173	4	1	6	304	322					
2	1	1	268	257	4	2	7	276	288	9	0	0	261	308
2	1	2	704	705	4	3	2	424	461	9	0	4	333	275
2	1	5	151	103	4	3	5	270	231					
2	1	6	471	419	4	3	8	238	193					
2	2	3	197	230	4	4	0	446	448					
2	2	4	199	208	4	4	2	234	192					
2	3	0	220	191	4	4	4	443	441					
2	3	1	317	326	4	4	5	221	160					
2	3	2	614	681	4	6	2	342	218					
2	3	6	413	446										
2	4	2	463	499	5	0	0	338	294					
2	4	3	459	451	5	0	3	280	305					
2	4	5	792	769	5	0	6	311	276					
2	4	6	428	445	5	0	7	328	272					
2	5	0	251	227	5	1	7	254	187					
2	6	7	316	299	5	2	0	318	316					

Appendix 4. The observed and calculated structure factors for phase A at 6.2 GPa

h	*k*	*l*	*Fo*	*Fc*	*h*	*k*	*l*	*Fo*	*Fc*	*h*	*k*	*l*	*Fo*	*Fc*
1	0	0	116	127	3	2	2	143	136	6	4	2	256	288
1	0	1	65	60	3	2	3	171	171					
1	1	0	520	473	3	3	0	186	169	7	0	2	304	261
1	1	1	366	407	3	3	1	311	268	7	0	3	322	313
1	1	2	153	181	3	3	2	194	175	7	1	0	323	304
1	2	2	1068	1028	3	3	3	234	276					
1	3	1	185	170	3	4	2	242	210					
1	3	2	398	377	3	5	3	231	224					
1	3	3	128	121	3	6	0	682	741					
1	4	0	401	444	3	7	2	212	205					
1	4	2	200	184										
1	4	3	255	248	4	0	0	242	275					
1	4	4	239	256	4	0	1	187	203					
1	6	0	235	236	4	0	2	217	254					
1	6	1	264	228	4	0	3	311	349					
1	6	2	462	453	4	1	0	1933	1890					
1	6	4	183	179	4	1	4	365	357					
1	8	2	224	231	4	2	2	238	274					
					4	3	2	392	376					
2	0	1	205	227	4	3	4	165	149					
2	0	2	621	713	4	4	0	381	382					
2	1	0	189	195	4	4	2	165	176					
2	1	1	277	254	4	4	4	361	335					
2	1	2	657	660	4	6	2	202	176					
2	2	1	223	221										
2	2	3	163	179	5	0	0	232	222					
2	3	0	221	230	5	0	3	221	215					
2	3	1	339	360	5	1	2	347	322					
2	3	2	626	650	5	2	0	272	259					
2	3	4	171	192	5	2	1	280	277					
2	4	2	436	470	5	2	3	313	297					
2	4	3	461	466	5	3	2	286	290					
2	4	4	389	384	5	3	3	296	295					
2	5	4	210	252	5	5	0	226	188					
2	7	0	225	193										
2	7	1	220	187	6	0	0	273	323					
					6	0	1	211	191					
3	0	0	475	436	6	0	3	240	252					
3	1	1	240	227	6	1	2	348	350					
3	1	3	295	319	6	1	3	198	200					
3	2	0	236	244	6	2	2	300	295					
3	2	1	212	213	6	4	0	220	180					

Appendix 5. The observed and calculated structure factors for phase A at 9.1 GPa

h	*k*	*l*	*Fo*	*Fc*	*h*	*k*	*l*	*Fo*	*Fc*	*h*	*k*	*l*	*Fo*	*Fc*
1	0	0	117	92	3	2	3	224	231	7	1	0	299	347
1	0	1	74	114	3	3	1	335	329					
1	1	0	481	445	3	3	2	161	199	8	2	0	604	680
1	1	1	361	482	3	3	3	269	302					
1	2	2	1051	1000	3	3	4	146	155	9	0	0	358	300
1	3	2	401	410	3	4	3	227	225					
1	4	0	458	517	3	5	1	259	188					
1	4	2	163	171	3	5	2	227	201					
1	4	3	226	249	3	5	3	270	243					
1	5	2	451	397	3	6	0	882	887					
1	6	1	234	277	3	7	2	273	231					
1	6	2	432	478										
1	6	3	235	222	4	0	0	255	306					
1	8	1	206	210	4	0	1	199	217					
1	8	2	296	267	4	0	2	226	250					
					4	0	3	336	372					
2	0	1	204	219	4	1	0	2080	2000					
2	0	2	644	698	4	1	4	409	404					
2	1	0	171	131	4	3	2	343	398					
2	1	1	267	285	4	4	2	197	157					
2	1	2	631	664	4	4	3	203	160					
2	2	1	217	244	4	5	0	241	183					
2	2	3	204	210	4	5	3	288	217					
2	3	0	239	228										
2	3	1	335	362	5	0	3	233	273					
2	3	2	649	650	5	1	2	365	296					
2	3	3	163	158	5	2	0	231	227					
2	3	4	185	168	5	2	3	284	302					
2	4	2	499	458	5	3	2	235	315					
2	4	3	558	547	5	3	3	334	326					
2	4	4	345	326	5	5	0	310	277					
2	5	0	261	214										
2	5	4	210	253	6	0	0	309	348					
2	7	0	287	260	6	0	1	240	256					
2	7	1	221	198	6	0	4	215	210					
					6	1	2	339	368					
3	0	0	468	454	6	2	2	365	326					
3	1	1	231	208	6	4	2	298	319					
3	1	3	325	333										
3	2	0	246	275	7	0	2	290	287					
3	2	1	165	192	7	0	3	325	338					
3	2	2	185	152	7	0	4	218	206					

Appendix 6. The observed and calculated structure factors for phase A at 9.4 GPa

h	*k*	*l*	*Fo*	*Fc*	*h*	*k*	*l*	*Fo*	*Fc*	*h*	*k*	*l*	*Fo*	*Fc*
1	0	0	106	108	2	4	6	486	419	5	1	2	384	262
1	0	1	76	62	2	5	0	248	201	5	2	0	232	243
1	0	2	174	197	2	6	7	312	286	5	2	1	307	282
1	0	3	304	364						5	2	3	310	319
1	1	0	444	444	3	0	0	435	425	5	2	7	291	316
1	1	1	381	381	3	0	4	391	399	5	3	2	300	319
1	1	2	164	204	3	1	3	331	345	5	3	3	367	329
1	1	3	432	464	3	1	6	241	244	5	3	4	242	246
1	2	2	1197	1083	3	2	0	243	220	5	3	5	558	556
1	2	3	970	964	3	2	2	165	143	5	3	6	306	316
1	2	4	677	678	3	2	3	234	246					
1	2	5	1234	1224	3	2	7	356	367	6	0	0	281	307
1	2	6	611	660	3	3	0	192	186	6	0	1	185	202
1	3	2	410	431	3	3	1	325	283	6	0	7	282	243
1	3	3	118	157	3	3	2	198	211	6	1	2	375	380
1	3	4	171	187	3	4	2	269	262	6	2	2	358	329
1	4	0	432	463	3	5	1	200	183	6	4	1	225	206
1	4	4	233	239	3	5	6	253	241	6	4	2	372	331
1	5	5	275	286	3	5	7	290	259					
1	5	7	210	180	3	6	0	876	904	7	0	2	250	308
1	6	0	198	182	3	6	4	232	225	7	0	3	376	333
1	6	2	407	476						7	0	4	285	262
1	6	6	325	304	4	0	0	283	273	7	0	5	545	558
1	8	2	265	296	4	0	1	196	165	7	0	6	343	301
					4	0	2	220	237	7	1	4	308	329
2	0	1	224	226	4	0	3	349	368	7	2	1	230	167
2	0	2	727	751	4	0	6	319	357					
2	0	4	238	225	4	1	0	2004	2018	9	0	0	366	294
2	1	1	277	268	4	1	4	427	431					
2	1	2	699	702	4	1	6	304	291					
2	2	1	235	226	4	2	7	218	213					
2	2	3	214	206	4	3	2	394	455					
2	2	4	206	214	4	3	5	247	224					
2	3	0	235	212	4	3	6	281	269					
2	3	1	322	335	4	4	0	362	425					
2	3	2	616	680	4	4	2	196	215					
2	3	4	182	182	4	4	4	337	333					
2	3	5	198	167	4	5	0	193	185					
2	3	6	403	436	4	5	6	227	233					
2	4	2	473	503										
2	4	4	401	397	5	0	0	217	229					
2	4	5	843	773	5	0	7	264	286					

Appendix 7. The observed and calculated structure factors for phase A at 10.8 GPa

h	*k*	*l*	*Fo*	*Fc*	*h*	*k*	*l*	*Fo*	*Fc*	*h*	*k*	*l*	*Fo*	*Fc*
1	0	0	118	101	3	1	1	217	215	5	3	2	320	332
1	0	1	45	47	3	1	2	138	162	5	3	3	329	338
1	1	0	486	446	3	1	3	307	366	5	3	4	188	230
1	1	1	351	391	3	2	0	215	231	5	4	2	193	178
1	1	2	151	192	3	2	1	159	163	5	5	0	304	263
1	2	2	1064	1070	3	2	3	224	239					
1	3	1	196	167	3	3	0	184	179	6	0	0	295	335
1	3	2	406	420	3	3	1	287	277	6	0	1	249	213
1	3	3	170	176	3	3	2	170	167	6	0	3	274	275
1	4	0	456	468	3	3	3	299	296	6	0	4	254	227
1	4	2	199	211	3	3	4	145	164	6	1	2	382	392
1	4	3	235	263	3	4	2	274	244	6	1	3	220	199
1	5	1	188	164	3	5	1	178	162	6	2	2	318	324
1	5	2	385	396	3	5	2	199	177	6	2	3	203	193
1	6	1	280	275	3	5	3	260	251	6	4	2	351	344
1	6	2	473	486	3	6	0	917	909					
1	6	3	203	193	3	6	4	227	213	7	0	2	323	313
1	8	2	320	293	3	7	2	245	214	7	0	3	346	350
										7	0	4	264	242
2	0	1	205	233	4	0	0	275	290	7	1	0	357	339
2	0	2	684	721	4	0	1	191	163	7	1	4	351	350
2	1	0	164	154	4	0	2	221	232	7	3	0	251	224
2	1	1	270	270	4	0	3	339	371					
2	1	2	626	666	4	1	0	2095	2013	8	2	0	660	699
2	2	0	228	180	4	1	4	395	406					
2	2	1	214	225	4	2	2	250	231	9	0	0	313	287
2	2	3	199	204	4	3	2	416	439					
2	3	0	223	178	4	4	0	357	424					
2	3	1	337	353	4	4	2	248	217					
2	3	2	649	674	4	4	4	352	370					
2	4	2	509	504	4	5	0	200	204					
2	4	3	489	510	4	5	3	161	187					
2	4	4	383	384	4	6	2	206	185					
2	5	0	211	223										
2	5	4	275	286	5	0	0	248	241					
2	6	0	176	168	5	0	3	265	257					
2	7	0	255	229	5	1	2	259	269					
2	7	1	219	172	5	1	3	156	164					
					5	2	0	228	248					
3	0	0	445	431	5	2	1	273	292					
3	0	2	210	236	5	2	3	290	312					
3	0	3	222	223	5	2	4	224	239					